Inter-Landau-Level Pair Tunneling Rigidifies the Long-Wavelength Structure Factor of the $\nu = 1/3$ Laughlin State

Hongyi LIU[1]

[1] *Westlake University*

(Dated: May 27, 2026)

A textbook chain of reasoning, originating with Girvin, MacDonald, and Platzman [Phys. Rev. B **33**, 2481 (1986)], predicts that Landau-level mixing (LLM) at $\nu = 1/3$ should soften the long-wavelength guiding-centre structure factor $S(L)$: virtual excitations to higher Landau levels suppress the short-range pseudopotential V_1, the magnetoroton gap Δ closes, and the single-mode approximation $\Delta \simeq f(L)/\bar{S}(L)$ then forces $\bar{S}(L)$ to increase. We test this chain in two complementary ways on the Haldane sphere at $\nu = 1/3$, $N = 6$, $2Q = 15$. (i) Perturbatively, by first-order Schrieffer–Wolff dressing of the lowest-Landau-level (LLL) Laughlin ground state into the second LL and same-LL pair sectors, fed the Löwdin-renormalised pseudopotentials. The dressed state gives $\Delta S(1)|_{\kappa=10} \simeq +21\%$, recovering both the sign and the magnitude predicted by the GMP chain (the $\sim 19\%$ softening of $V_1^{\rm eff}$). (ii) Non-perturbatively, by rigorous two-Landau-level (LLL$\oplus$SLL) exact diagonalisation using a repaired implementation of the DiagHam 2LL module that, for the first time on the sphere, retains the full set of inter-LL scattering channels. Here the response reverses sign: $S(1)$ *rigidifies* monotonically from 0.118 at $\kappa \to 0$ to 0.080 at $\kappa = 10$, a 32% suppression. The leading-order perturbative result and the non-perturbative result therefore disagree in sign, with a combined gap of ~ 53 percentage points between $+21\%$ (SW) and -32% (full ED). A runtime channel-mask ablation localises the entire reversal to a single Hermitian inter-LL pair, the DD↔UU pair-tunneling channel, which alone reproduces 98% of the full shift; the remaining five inter-LL channels contribute at the 10^{-3} level. A four-way decomposition (Löwdin LLL-ED on the LLL attractor, first-order SW dressing into the 2LL space, and the 2LL ED with the channel disabled vs. retained on the same 2LL Hilbert space) shows that the two-body content of this channel is kinematically frozen on the LLL Laughlin attractor, its first-order perturbative inter-LL admixture pulls $S(1)$ in the GMP direction, and its three-body and higher coherent content overpowers that admixture by a factor $\sim 2.5\times$ in the opposite direction. The mechanism is structurally distinct from the three-body residuals invoked at $\nu = 5/2$: it is a coherent pair-tunneling process between the LLL and SLL whose two-body and many-body parts cancel and reinforce in opposite senses on $S(1)$. The same channel diagnostic provides a calibration handle for variational ansätze that operate within the LLL Laughlin basin: a recent neural-network ansatz reproduces the monotonic decrease of $S(1)$ with κ and sits within 5–8% of the 2LL ED across the full range.

I. INTRODUCTION

The fractional quantum Hall (FQH) effect [1–4] is the canonical example of a strongly correlated topological state. The clean theoretical control afforded by Haldane's spherical geometry [3], combined with the universality of the Laughlin wavefunction at filling $\nu = 1/p$ for odd p, has made the $\nu = 1/3$ state the textbook testing ground for analytical and numerical methods. In this setting, Landau-level mixing (LLM) – the deviation from strict lowest-Landau-level (LLL) projection at finite cyclotron-to-Coulomb ratio $\kappa = (e^2/\epsilon\ell_B)/\hbar\omega_c$ – is widely regarded as a benign, perturbative correction: the Laughlin state is robust, and LLM is expected only to renormalise quantitative details without disturbing the qualitative incompressible-liquid picture [5–8].

A long-standing inferential chain, sometimes called the GMP folklore, sharpens this expectation into a quantitative prediction for the long-wavelength density response. The chain has three links:

(i) LLM softens the short-range pseudopotential $V_1^{\rm eff}(\kappa)$ through virtual excitations to higher Landau levels [9–15];

(ii) The magnetoroton gap Δ is set by V_1 through Haldane's hard-core argument, $\Delta \propto V_1$;

(iii) The single-mode approximation [16, 17] relates the gap to the LLL-projected guiding-centre structure factor, $\Delta_{\rm SMA}(L) = f(L)/\bar{S}(L)$, with $f(L)$ weakly sensitive to the pseudopotentials.

The composition predicts $V_1^{\rm eff} \downarrow \Rightarrow \Delta \downarrow \Rightarrow \bar{S}(L) \uparrow$ – a softening of long-wavelength density fluctuations whose magnitude tracks the $\sim 19\%$ pseudopotential softening at $\kappa = 10$.

Despite its central place in textbook reasoning about LLM at $\nu = 1/3$, this chain has, to our knowledge, never been tested non-perturbatively against a multi-Landau-level exact diagonalisation (ED) on the sphere with the full inter-LL scattering channel set retained. Multi-LL studies on the sphere have historically either restricted the Hilbert space to the LLL with Löwdin-renormalised two-body pseudopotentials [10–12, 18–22], or moved to torus or cylinder geometries with multi-LL truncated Fock spaces [23–25], or used early sphere LLM treatments that did not retain the full set of inter-LL channels [26, 27]. The unprojected structure factor has, in

particular, never been measured under genuine multi-LL sphere ED.

In this paper we close this gap, and report a result that runs opposite to the GMP-chain prediction.

a. Result. Performing rigorous two-Landau-level (LLL⊕SLL) exact diagonalisation at $N = 6$, $2Q = 15$ ($\nu = 1/3$, Laughlin shift) using a repaired implementation of the DiagHam [28, 29] 2LL module that for the first time retains all six inter-LL scattering channels, we find that the long-wavelength structure factor $S(1)$ *decreases* monotonically with κ, from 0.118 at $\kappa = 10^{-2}$ to 0.080 at $\kappa = 10$. This is a 32% *rigidification* of long-wavelength density fluctuations, opposite in sign to the $\sim 19\%$ enhancement predicted by the GMP-chain reasoning. Sec. III traces the failure to step (iii): a Löwdin two-body downfolding to the LLL, fed with the same softened $V_m^{\rm eff}(\kappa)$ and operating on the same Hilbert space as a strict-LLL ansatz, gives $\Delta S(1) = 0$ exactly across the full κ range. This identifies the chain's failure as a structural property of two-body downfolding – the standard analytic vehicle for incorporating LLM into LLL-projected calculations – rather than a deficiency of the SMA itself, and isolates the missing physics as inter-LL many-body coherence that no two-body effective Hamiltonian on the LLL can carry.

A runtime channel-mask ablation (Sec. VI) sharpens this further: the rigidification is generated by a single Hermitian inter-LL pair, the DD↔UU pair-tunneling channel that we label **AB**. AB alone reproduces 98% of the full $\Delta S(1)$; the remaining five inter-LL channels combined contribute at the 10^{-3} level. A four-way decomposition (Sec. VII) – Löwdin LLL-ED, first-order SW dressing, 2LL ED with AB off, and full 2LL ED – shows that the two-body component of AB contributes exactly zero to $\Delta S(1)$; the first-order SW dressing gives $\Delta S(1)|_{\kappa=10} = +0.025$ in the GMP direction; and the entire 32% shift is carried by the three-body and higher coherent component that overpowers the perturbative admixture by $\sim 2.5\times$ in the opposite direction.

b. Relation to prior multi-LL ED results. The general statement that two-body downfolding does not exhaust the LLM-induced effective Hamiltonian is not new. At $\nu = 5/2$, Rezayi [25] demonstrated that the two-body Bishara–Nayak [10], Sodemann–MacDonald [11], and Simon–Rezayi [12] effective Hamiltonians miss a critical higher-order term whose inclusion is decisive for the Pf-vs-aPf phase competition; subsequent work [19, 30–32] has refined that picture. The present work is concerned with a filling, an observable, and a microscopic mechanism that are all distinct from this $\nu = 5/2$ literature. (i) *Filling.* We work at $\nu = 1/3$, where LLM is generally regarded as benign and the Laughlin state robust; the GMP-chain prediction is that LLM should produce a small $\sim 19\%$ *enhancement* of $S(L)$, not a sign-reversed effect. (ii) *Observable.* We measure the unprojected guiding-centre $S(L)$ and its κ-derivative, not the energy splitting between candidate paired ground states. (iii) *Mechanism.* The decisive process is a single Hermitian inter-Landau-level pair-tunneling channel DD↔UU whose two-body component is identically zero on $\Delta S(1)$, whose first-order perturbative (SW) inter-LL admixture gives $\Delta S(1) > 0$ in the GMP direction, and whose three-body-and-higher coherent component overpowers that admixture by $\sim 2.5\times$ in the opposite direction; this is structurally different from the three-body *residual* (Hartree-Fock-like correction to the bare two-body interaction) discussed in the $\nu = 5/2$ literature. We do not recover Rezayi's $\nu = 5/2$ result at a different filling; we identify a structurally distinct multi-body signature of LLM at a filling where no such signature was previously expected.

c. Outline. Sec. II fixes geometry, kinematic conventions, and the definition of $S(L)$. Sec. III constructs the Löwdin two-body downfolding and exhibits its κ-independence on $S(1)$. Sec. IV summarises the repair of the DiagHam 2LL module that enables the rigorous benchmark; full details are reserved for a companion software paper. Sec. V reports the rigorous 2LL ED result for $S(1, \kappa)$. Sec. VI performs the channel-mask ablation that localises the response to AB. Sec. VII carries out the four-way decomposition that isolates the perturbative vs. non-perturbative many-body content of AB. Sec. X discusses physical interpretation, the relationship to the $\nu = 5/2$ literature, and implications for variational ansätze.

II. SETUP AND CONVENTIONS

We consider N spinless fermions on the Haldane sphere of radius $R = \sqrt{Q}\,\ell_B$ pierced by a monopole of strength $2Q$. Single-particle states are monopole harmonics $|n, m\rangle$ with $n = 0, 1, \ldots$ the Landau-level index and $m = -(Q + n), \ldots, (Q + n)$ the angular-momentum projection. The two-Landau-level (2LL) truncation retains $n = 0$ (LLL, "D") and $n = 1$ (SLL, "U"), giving $N_{\rm orb} = (2Q + 1) + (2Q + 3) = 4Q + 4$ orbitals. At $N = 6$, $2Q = 15$, $N_{\rm orb} = 34$.

The single-particle gap on the sphere is the exact monopole-harmonic value $\varepsilon_n - \varepsilon_0 = [(Q + n)(Q + n + 1) - Q(Q + 1)]/(2Q)\,\hbar\omega_c$, which fixes the SLL kinetic cost at $(Q + 1)/Q\,\hbar\omega_c = (17/15)\,\hbar\omega_c$ for $2Q = 15$. We parametrise the relative strength of Coulomb to cyclotron energy by $\kappa = (e^2/\epsilon\ell_B)/\hbar\omega_c$.

The unprojected sphere structure factor at angular momentum L is $S(L) = N^{-1}\langle\sum_{i\neq j} P_L(\cos\gamma_{ij})\rangle$, where P_L is the Legendre polynomial and γ_{ij} is the geodesic angle between particles i and j. For the LLL Laughlin state at $N = 6$, $2Q = 15$, $S(1) = 1/(Q + 1) = 0.11765$ exactly. $S(L)$ obeys the Pauli sum rule $\sum_L (2L+1)\,S(L) = N_{\rm orb} - N = 28$, which we verify to machine precision in every calculation reported below.

a. Absence of a variational inequality on $S(L)$. We emphasise at the outset that no variational inequality constrains $S(L)$ analogous to the Rayleigh–Ritz upper bound on the energy: an LL truncation that lowers (or raises) $S(1)$ does so as an empirical fact, not by theorem, and the same holds for any approximate wavefunction rel-

ative to the exact ground state. The internal consistency of the 2LL benchmark reported below therefore does not rely on a convergence claim with respect to higher Landau levels. It rests instead on two structural diagnostics that operate *within* the shared LLL⊕SLL Hilbert space: the runtime channel-mask ablation (Sec. VI) that localises the entire response to a single Hermitian inter-LL pair, and the truncation-independent four-way decomposition (Sec. VII) that separates the two-body, perturbative inter-LL, and non-perturbative many-body content of the AB channel. All quantitative comparisons to other methods are framed below as empirical calibration, not as upper or lower bounds.

A definitional remark is in order. Three closely related objects appear in the LLM literature: (i) the LLL-projected guiding-centre structure factor $\bar{S}(L)$ that enters the GMP single-mode approximation; (ii) the unprojected structure factor evaluated on the 2LL-truncated many-body wavefunction (the LLL⊕SLL Hilbert space of the rigorous ED reported below); and (iii) the unprojected structure factor evaluated on a wavefunction defined on the full single-particle space (as computed by neural-network MCMC in Ref. [33]). Definitions (ii) and (iii) differ by cross-LL terms weighted by SLL occupation; the magnitude of this correction is bounded below. Throughout this paper, "$S(L)$" without further qualification refers to definition (ii).

b. Magnitude of the (ii)→(iii) cross-LL correction. The 2LL ED reports definition (ii) (unprojected $S(L)$ on the LLL⊕SLL Hilbert space), while neural-network MCMC computes definition (iii) (unprojected $S(L)$ on the full single-particle space, with no LL truncation). The two differ by cross-LL contributions weighted by the $n \geq 2$ occupation. At the production size $(N, 2Q) = (6, 15)$ and $\kappa \leq 1$, the SLL occupation per particle is $\langle n_{\mathrm{SLL}} \rangle / N \lesssim 0.05$ and the (ii)→(iii) correction to $S(1)$ is bounded at the few-percent level. The 2LL→3LL→4LL ladder of Sec. IX brackets the residual to even finer precision: at $\kappa \leq 1$ the 4LL − 3LL shift on $S(1)$ at $(N, 2Q) = (4, 9)$ is $\leq 4 \times 10^{-4}$. The (ii)/(iii) offset is therefore quantitatively bounded at small and intermediate κ and cannot account for any observed discrepancy at the 5% level or larger in that regime. At the large-κ end ($\kappa \gtrsim 5$) the SLL occupation per particle rises and the few-percent bound on the (ii)/(iii) gap is correspondingly less tight; we therefore do not rely on the (ii)/(iii) bound alone at $\kappa = 10$, and the diagnostic statements in Sec. X that compare to external full-space wavefunctions are framed as empirical patterns calibrated against the within-2LL channel-mask consistency, not against the (ii)/(iii) gap.

III. LÖWDIN TWO-BODY DOWNFOLDING AND THE GMP FOLKLORE

We first construct an analytically transparent benchmark using the Löwdin downfolding to the LLL, which is the leading-order limit of the broader effective-Hamiltonian programme initiated by Rezayi and Haldane [9] and refined in Refs. [10–12, 18, 19].

TABLE I. Löwdin-downfolded effective LLL pseudopotentials $V_m^{\mathrm{eff}}(\kappa)$ in units of $e^2/(\epsilon \ell_B)$ at $2Q = 15$, for the full κ range used in this work.

κ	V_1	V_3	V_5	V_7	V_9	V_{11}
10^{-6}	0.47810	0.30921	0.25261	0.22371	0.20678	0.19656
0.1	0.47670	0.30899	0.25253	0.22368	0.20677	0.19655
0.5	0.47106	0.30811	0.25224	0.22355	0.20671	0.19652
1.0	0.46406	0.30702	0.25187	0.22340	0.20664	0.19649
3.0	0.43811	0.30281	0.25046	0.22279	0.20636	0.19636
5.0	0.41756	0.29893	0.24912	0.22221	0.20609	0.19624
10.0	0.38607	0.29083	0.24611	0.22089	0.20547	0.19594

TABLE II. Coulomb energy per particle E_c/N from three methods at $N = 6$, $2Q = 15$, $\nu = 1/3$ (units $e^2/\epsilon \ell_B$).

κ	LLL ED (bare)	DeepHall NN	Löwdin 3×3
10^{-6}	−0.410950	—	−0.410950
0.1	−0.410950	—	−0.411205
0.5	−0.410950	−0.411056	−0.412221
1.0	−0.410950	−0.411645	−0.413479
3.0	−0.410950	−0.413331	−0.418339
5.0	−0.410950	—	−0.422852
10.0	−0.410950	−0.417425	−0.432396

For each relative angular momentum m, the two-body two-LL Hamiltonian acts on the basis $\{|LL; m\rangle, |SL; m\rangle, |SS; m\rangle\}$ as a 3×3 matrix in which the diagonal entries include the SLL kinetic cost: $|SL\rangle$ contributes $(Q+1)/Q\,/\kappa$ and $|SS\rangle$ contributes $2(Q+1)/Q\,/\kappa$ in units of $e^2/\epsilon \ell_B$. Diagonalising and taking the lowest eigenvalue yields an effective LLL pseudopotential $V_m^{\mathrm{eff}}(\kappa)$. Table I reports $V_m^{\mathrm{eff}}(\kappa)$ across the full κ range used in this work.

All six V_m^{eff} decrease monotonically with κ: V_1 drops by $\sim 19.3\%$ between $\kappa = 10^{-6}$ and $\kappa = 10$, V_3 by 4.5%, and the softening fades to 0.3% at V_{11}. Virtual excitations to the SLL screen the short-range Coulomb repulsion, weakening the hard-core component V_1 that stabilises the Laughlin state. Step (i) of the GMP chain is therefore quantitatively confirmed at the two-body level.

We also report, in Table II, the Löwdin-LLL ED Coulomb energy per particle as a function of κ, benchmarked against the bare-LLL ED energy and the DeepHall neural network value of Ref. [33]. The Löwdin energy systematically deviates downward from the bare LLL: it captures the leading two-body softening but overcounts virtual excitations because the truncation discards the $\geq$ 3-body counterterms, and the discrepancy grows from $\sim 3 \times 10^{-4}$ at $\kappa = 0.1$ to $\sim 2.1 \times 10^{-2}$ at $\kappa = 10$. The Löwdin two-body downfolding is therefore a controlled approximation only for $\kappa \lesssim 1$; at $\kappa \geq 3$ the rigorous 2LL ED of Sec. V is required as a benchmark.

The chain then predicts: a 19% drop in V_1^{eff} should

imply a comparable drop in Δ via Haldane's hard-core argument, which through the SMA

$$\Delta_{\mathrm{SMA}}(L) \;=\; \frac{f(L)}{\bar{S}(L)} \tag{1}$$

should produce a comparable $\sim 19\%$ *increase* in $\bar{S}(1)$.

We test this prediction directly. Using $V_m^{\mathrm{eff}}(\kappa)$ from Table I as input to a standard $N = 6$ LLL exact diagonalisation (Hilbert-space dimension 338 in the $L_z = 0$ sector), we find $S(1) = 0.11765$ *independent of* κ *across all seven values* $\kappa \in [10^{-6}, 10]$, agreeing with the LLL Laughlin value to machine precision. The V_1 softening does not propagate to $S(1)$.

We emphasise that this $\Delta\bar{S}(1) = 0$ is not by itself a failure of the GMP chain: it is instead a *kinematic* property of the LLL Laughlin attractor, which blocks the chain at step (iii) because the wavefunction is strictly LLL-projected. The proper perturbative implementation — first-order Schrieffer–Wolff dressing of the LLL state into the SLL/SS sectors (row (a′) of Sec. VII) — does move $S(1)$, and does so in the GMP-predicted direction ($\Delta S(1)|_{\kappa=10} \approx +0.025$, i.e. $\approx +21\%$ of the Laughlin value).

The Löwdin downfolding is, however, only a benchmark for what a two-body treatment of LLM predicts without inter-LL admixture. In Sec. V we will show that the rigorous many-body 2LL ED, fed with the *same underlying pseudopotential input*, gives a qualitatively different answer: $S(1)$ does respond to κ, and in the opposite direction from the GMP-chain prediction. The four-way decomposition developed in Sec. VII – comparing the Löwdin LLL-ED, the first-order SW-dressed state, the 2LL ED with AB off, and the full 2LL ED, all sharing the same Hilbert space and pseudopotential input – is the truncation-independent core of this paper.

IV. REPAIRED DIAGHAM 2LL MODULE: SUMMARY

The rigorous 2LL ED reported in this paper requires the full two-Landau-level Hamiltonian on the sphere, including all inter-Landau-level scattering channels and the full 10-channel pseudopotential structure $V_m^{(n_1 n_2; n_3 n_4)}$ derived from the bare Coulomb interaction with monopole-harmonic single-particle wavefunctions. We use a repaired implementation of the DiagHam [28, 29] 2LL module (`ParticleOnSphereTwoLandauLevelHamiltonian`); the analytic Schrieffer–Wolff/Löwdin machinery underlying the comparison two-body downfolding follows the standard formulation reviewed in Ref. [34]. In the course of this work we identified nine issues that collectively rendered the existing module incomplete. We document them here briefly to substantiate the repaired benchmark; full implementation details and the regression-test suite are reserved for a companion software publication.

TABLE III. Unprojected structure factor $S(L)$ from the rigorous 2LL ED at $N = 6$, $2Q = 15$. The $\kappa = 0.01$ to $\kappa = 10$ ratio at $L = 1$ is $S(1)|_{\kappa=0.01}/S(1)|_{\kappa=10} = 1.48$ (i.e. a 32% rigidification).

L	$\kappa = 0.01$	$\kappa = 1$	$\kappa = 3$	$\kappa = 10$
1	0.11755	0.10902	0.09707	0.07973
2	0.35058	0.32892	0.29949	0.25675
3	0.67058	0.66632	0.65757	0.63675
4	0.84114	0.87487	0.91938	0.98096
5	0.54919	0.54451	0.53607	0.52053
6	0.29256	0.28515	0.27613	0.26458
7	0.14070	0.13892	0.13755	0.13792
8	0.06109	0.06198	0.06404	0.06907

In total we identified nine distinct issues, the most consequential of which (#7) is the complete absence of six inter-LL scattering channels labelled A–F (`DD`↔`UU`, `UD`↔`UU`, `UD`↔`DD`). The repaired module reproduces, to 11 significant digits, the LLL ED energy in the $\kappa \to 0$ limit; saturates the Pauli sum rule $\sum_L (2L{+}1)\, S(L) = N_{\mathrm{orb}} - N$ to machine precision at every κ on the production system $(N, 2Q) = (6, 15)$ (Appendix C); and passes a suite of 17 regression tests at $(N, 2Q) = (2, 3), (4, 9), (6, 15)$. The full bug list, the per-channel fermionic prefactors, and the parity-filtering rule for the pseudopotentials are documented in Appendix A.

We emphasise that the very small number of published works that have extended exact diagonalisation to two Landau levels on the Haldane sphere makes it likely that the practical impact of these bugs on the published literature is limited. The repaired module is offered primarily as an enabling tool for future multi-LL studies, not as a critique of any specific prior result.

V. RIGOROUS 2LL EXACT DIAGONALISATION: $S(1)$ RIGIDIFIES

Using the repaired DiagHam 2LL module, we perform full exact diagonalisation of the $N = 6$, $2Q = 15$ system across seven values of $\kappa \in \{10^{-2}, 10^{-1}, 0.5, 1, 3, 5, 10\}$ in the $L_z = 0$ sector. The Hilbert-space dimension is 47 044.

Table III reports the unprojected $S(L)$ for $L = 1, \ldots, 8$ at the four representative κ values; the full spectrum at $L = 1, \ldots, 14$ saturates the Pauli sum rule $\sum_L (2L + 1)\, S(L) = 28$ to machine precision at every κ.

The central finding is that $S(1)$ *decreases* monotonically with κ, from 0.118 at $\kappa = 10^{-2}$ (in agreement with the LLL Laughlin value $1/(Q + 1) = 0.11765$) to 0.080 at $\kappa = 10$, a 32% rigidification of long-wavelength density fluctuations. The same trend holds for $L = 2$ (-27%), is weaker but same-sign for $L = 3$ (-5%), and reverses sign for $L \geq 4$, where the spectral weight is redistributed toward higher angular momentum (the isosbestic-redistribution pattern enforced by the Pauli sum rule).

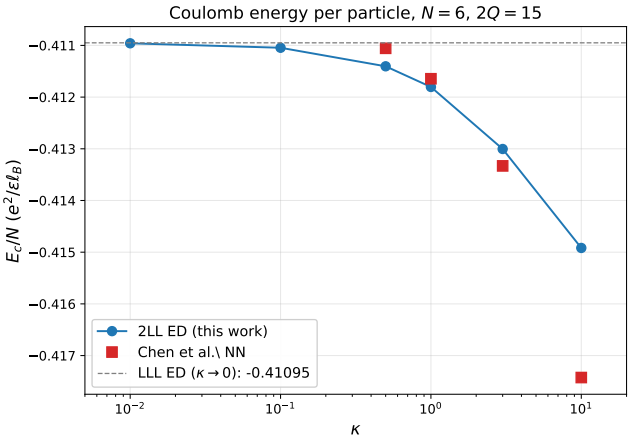

FIG. 1. Coulomb energy per particle E_c/N vs κ at $N = 6$, $2Q = 15$ from the rigorous 2LL ED. The horizontal dashed line is the $\kappa \to 0$ LLL ED reference. The energy decreases monotonically with κ as expected for a constrained variational principle in which higher Landau levels are added.

TABLE IV. The three Hermitian pairs of inter-LL scattering channels restored by the repair. "D" denotes a LLL orbital, "U" a SLL orbital.

pair	process	physical content
AB	DD↔UU	LLL pair ↔ SLL pair (pair tunneling)
CD	UD↔UU	single-LLL→SLL hop with U spectator
EF	UD↔DD	single-SLL→LLL hop with D spectator

This direction is opposite to the GMP-chain prediction of Sec. III ($\sim 19\%$ enhancement of $S(1)$), and the magnitude is much larger. The rigorous many-body treatment within the 2LL Hilbert space gives an answer of qualitatively different character from the Löwdin two-body downfolding within the same space.

VI. CHANNEL-MASK ABLATION: AB CARRIES THE RIGIDIFICATION

The repair of Sec. IV restores six inter-Landau-level scattering channels, organised into three Hermitian pairs. Following the labelling of Table IV, we call these pairs **AB**, **CD**, and **EF**.

To localise the channel responsible for the rigidification observed in Sec. V, we introduce a runtime channel-mask variable `CHANNEL_MASK`, a 6-bit integer in which bit i enables one of the six inter-LL channels. Hermiticity restricts attention to eight values in which each pair is fully on or fully off. We perform a 48-point ablation over 8 masks and 6 values of κ at $N = 6$, $2Q = 15$. The full unmasked binary is bit-for-bit reproduced by `CHANNEL_MASK` $= 63$ (all six channels on).

Table V and Fig. 2 support four sharply localised statements.

a. (i) AB alone captures essentially the full shift. Comparing the "all on" mask 63 with "AB only" mask 3, $\Delta S(1)|_{\kappa=1}$ goes from -0.00853 to -0.00846, i.e. AB alone reproduces 99.2% of the full shift at the physical point. At $\kappa = 10$ the ratio is 98.0%.

b. (ii) Removing AB suppresses the shift to the 10^{-3} level. With AB disabled (mask 60 = CD+EF), $|\Delta S(1)| \le 5 \times 10^{-4}$ across the full κ range – three orders of magnitude below the effect with AB present.

c. (iii) CD alone is numerically inert at this filling/sector. Mask 12 (CD only) is bit-for-bit identical to mask 0 (none) at every κ, indicating that the CD matrix elements have vanishing overlap with any state reachable from the $L_z = 0$ ground state at this filling.

d. (iv) EF produces a small sub-percent shift not strictly additive with AB. Mask 48 (EF only) gives $|\Delta S(1)|_{\kappa=10}| = 1.2 \times 10^{-3}$, $\sim 3\%$ of the full shift. Mask 51 (AB+EF) exceeds the unmasked value by $\sim 9\%$, indicating a mild anti-correlation between EF and CD in the coherent sum rather than strict channel additivity.

e. Robustness across topological sectors. Repeating the full 48-point ablation at the quasiparticle and quasihole shifts $2Q = 14$ and $2Q = 16$ (still $N = 6$, $L_z = 0$) preserves the AB-dominance pattern: masks containing AB produce $|\Delta S(1)|_{\kappa=10}| \in [0.033, 0.048]$ across all three shifts, masks without AB stay below 0.016, and the sign is negative (rigidification) in every case. The hierarchy is robust to whether one sits exactly on the incompressible point.

f. Real-space cross-check. The same conclusion can be re-derived from the real-space pair correlator $f(\theta) \equiv \sum_{L\ge1}(2L+1)\,S(L)\,P_L(\cos\theta)$. At the correlation-hole scale $r/\ell_B \approx 1$, AB-containing masks produce a deepening of the correlation hole by $|\Delta f| \in [0.20, 0.37]$ at $\kappa = 10$, while non-AB masks give $|\Delta f| \le 0.04$ – a factor of 5–10 separation in the real-space signal, consistent in sign and magnitude with the momentum-space observation (Fig. 3).

The weak version of the result is therefore: *at $N = 6$, $L_z = 0$, and across three consecutive monopole-flux sectors $2Q \in \{14, 15, 16\}$, the AB pair-tunneling channel (DD↔UU, mediated by the $m = 1$ pseudopotential) dominates the κ-induced rigidification of $S(1)$, and the other two inter-LL pairs produce effects that are at most $\sim 30\%$ of the AB contribution and typically an order of magnitude smaller.*

VII. FOUR-WAY DECOMPOSITION: MANY-BODY CONTENT OF AB

Sec. III showed that the Löwdin two-body downfolding gives $\Delta S(1) = 0$. Sec. VI showed that the *full* 2LL ED with the AB channel disabled gives $\Delta S(1) \le 5 \times 10^{-4}$. The full 2LL ED with AB on gives $\Delta S(1)|_{\kappa=10} = -3.79 \times 10^{-2}$, a 32% suppression of the LLL Laughlin value. We now combine these three calculations — together with a fourth, the first-order Schrieffer–Wolff (SW) dressing of

TABLE V. Channel-mask ablation at $N = 6$, $2Q = 15$, $L_z = 0$. $\Delta S(1) \equiv S(1)|_\kappa - S(1)|_{\kappa=0.01}$ at the same mask. The "AB only" mask (mask 3) reproduces 98–99% of the full $\Delta S(1)$ of the unmasked binary at every κ; masks that exclude AB (masks 0, 12, 48, 60) leave $|\Delta S(1)| \leq 0.0013$ across the full range.

mask	channels	$E_c/N\,(\kappa=1)$	$S(1)\|_{\kappa=1}$	$\Delta S(1)\|_{\kappa=1}$	$E_c/N\,(\kappa=10)$	$S(1)\|_{\kappa=10}$	$\Delta S(1)\|_{\kappa=10}$
63	AB+CD+EF (all)	−0.41180	0.10902	−0.00853	−0.41492	0.07973	−0.03782
0	none	−0.41095	0.11765	0.00000	−0.41095	0.11765	0.00000
3	AB only	−0.41165	0.10909	−0.00846	−0.41419	0.08047	−0.03708
12	CD only	−0.41095	0.11765	0.00000	−0.41095	0.11765	0.00000
48	EF only	−0.41108	0.11760	−0.00005	−0.41143	0.11642	−0.00123
15	AB+CD	−0.41165	0.10910	−0.00845	−0.41433	0.08170	−0.03585
51	AB+EF	−0.41182	0.10897	−0.00858	−0.41547	0.07644	−0.04111
60	CD+EF (no AB)	−0.41108	0.11761	−0.00004	−0.41142	0.11716	−0.00049

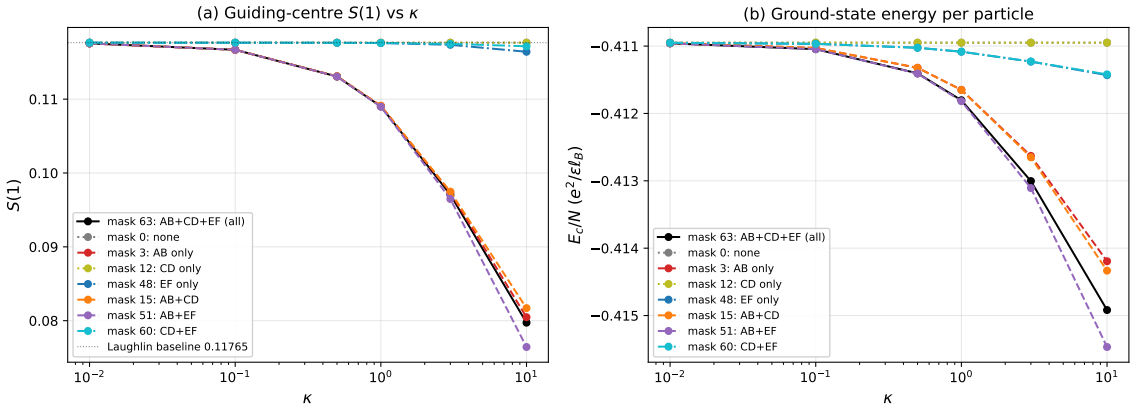

FIG. 2. Channel-mask ablation summary. (a) $S(1)$ vs κ for all eight masks. The pure-LLL Laughlin value 0.11765 is the horizontal dashed line. Masks containing AB form one family that falls by ~ 0.04 between $\kappa = 0.01$ and $\kappa = 10$; masks without AB stay within 1.5×10^{-3} of the Laughlin value. (b) Ground-state energy per particle E_c/N for the same runs.

the LLL state into the SLL/SS sectors — into a single decomposition that isolates the two-body, perturbative inter-LL, and non-perturbative many-body content of the AB process.

The four rows of Table VI are constructed so that each successive row adds exactly one piece of physics relative to the previous row, all four rows sharing the same bare Coulomb pseudopotentials on the LLL⊕SLL Hilbert space:

- Row (a) is the Löwdin two-body downfolding solved entirely within the LLL. It folds the AB two-body matrix elements into $V_m^{\rm eff}(\kappa)$ via virtual SLL pair excitation, giving the $\sim$ 19% softening of $V_1^{\rm eff}$ at $\kappa = 10$ (Table I). The many-body wavefunction is, however, strictly LLL: no SLL/SS admixture is permitted. Within that constraint $\Delta S(1) = 0$ is a kinematic identity of the LLL Laughlin attractor.

- Row (a′) takes the same LLL ground state $|\psi\rangle$ of row (a) and adds first-order Schrieffer–Wolff dressing, $|\psi\rangle \to |\psi\rangle + S|\psi\rangle$, where S is the generator that decouples the LLL block from the SLL/SS blocks at leading order. This is the textbook analytic implementation of the GMP chain. The dressed state lives in the full LLL⊕SLL Hilbert space.

- Row (b) is the full 2LL ED with the AB channel masked off (`CHANNEL_MASK` = 0 or 60). It excludes AB at all orders (two-body, three-body, and higher) while retaining the four remaining inter-LL channels.

- Row (c) is the full 2LL ED with AB on. It contains AB at all orders, including three-body and higher coherent contractions.

Rows (a) and (b) agree to better than 10^{-4} at every κ. This agreement is decisive. Row (a) contains the two-body part of AB through $V_m^{\rm eff}(\kappa)$ (with a $\sim$ 19% softening of $V_1^{\rm eff}$ at $\kappa = 10$) but is kinematically frozen on the LLL Laughlin attractor; row (b) lives on the full LLL⊕SLL Hilbert space but contains no AB at any order. That they give the *same* $\Delta S(1) = 0$ shows that on a quantum dynamics that forbids inter-LL pair tunneling — whether by Hilbert-space restriction (a) or by Hamiltonian restriction (b) — the $V_1^{\rm eff}$ softening cannot register as a $\Delta S(1)$.

Row (a′) is the proper perturbative GMP-chain test. It removes the kinematic restriction of (a) by dressing the

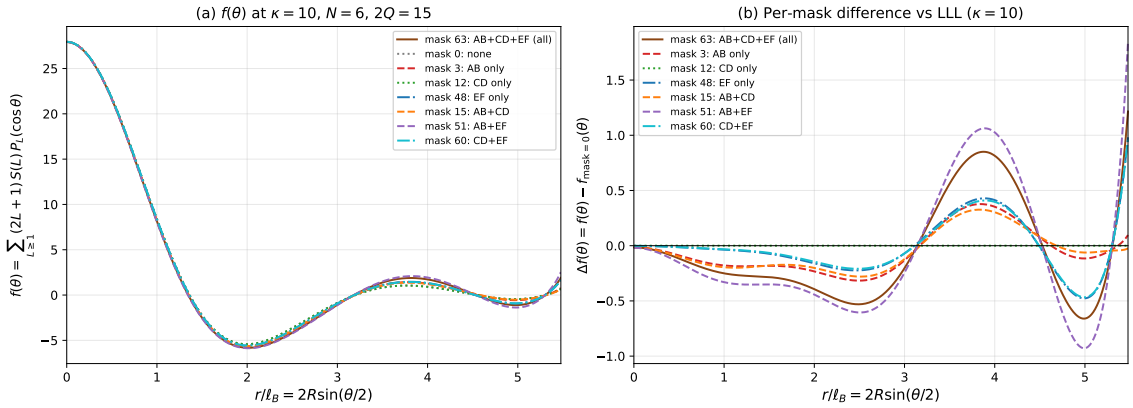

FIG. 3. Real-space pair-correlation deviation $f(\theta) = \sum_{L\geq 1}(2L+1)\,S(L)\,P_L(\cos\theta)$ at $\kappa = 10$, all eight masks. AB-containing masks produce a clear deepening of the correlation hole at $r/\ell_B \approx 1$; non-AB masks remain flat. Same physics as Fig. 2, in real space.

TABLE VI. Four-way decomposition of the κ-induced $S(1)$ response. (a) is the Löwdin two-body downfolding (no SW dressing). (a′) adds first-order Schrieffer–Wolff dressing of the LLL ground state into the SLL/SS sectors, $|\psi\rangle \to |\psi\rangle + S|\psi\rangle$, which retains the leading inter-LL admixture at the perturbative level. Agreement of (a) and (b) shows that the two-body content of AB contributes exactly zero to $\Delta S(1)$ within the LLL; (a′) captures the same direction as the perturbative GMP chain but with the wrong sign relative to the full 2LL ED (c). The entire non-perturbative response is carried by the three-body and higher coherent component that only (c) retains.

method	$S(1)\|_{\kappa=1}$	$S(1)\|_{\kappa=10}$	$\Delta S(1)\|_{\kappa=10}$
(a) Löwdin LLL-ED	0.11765	0.11765	0.00000
(a′) + 1st-order SW dress	0.12229	0.14248	+0.02483
(b) 2LL ED, AB off	0.11765	0.11765	0.00000
(c) 2LL ED, AB on (full)	0.10902	0.07973	−0.03792

LLL ground state into the SLL/SS sectors at leading order. The SW-dressed $\Delta S(1)|_{\kappa=10} = +0.025$ recovers the sign of the GMP chain ($\bar{S}(L) \uparrow$ under LLL softening) at a magnitude commensurate with the underlying $\sim 19\%$ softening of V_1^{eff}.

Row (c) is qualitatively different: $\Delta S(1)|_{\kappa=10} = -0.038$, a 32% rigidification. Row (c) differs from row (b) only in that AB is now retained at *all* orders, including three-body and higher coherent contractions. The difference $\Delta S(1)_{(c)} - \Delta S(1)_{(a')} = -0.038 - (+0.025) = -0.063$ shows that the non-perturbative coherent many-body content overpowers the perturbative admixture by a factor $\sim 2.5\times$ in the *opposite* direction.

a. Hierarchy reversal. The Löwdin two-body downfolding incurs a $\sim 0.6\%$ error on the energy ($|\Delta E_c/N| \approx 2.5 \times 10^{-3}$ at $\kappa = 1$, $\sim 2.1 \times 10^{-2}$ at $\kappa = 10$), but a 32% error on $S(1)$ at $\kappa = 10$. The many-body part of AB is far more important for the long-wavelength density correlator than for the total energy. This is the inverse of the usual hierarchy in which the energy is the most sensitive observable.

b. Truncation independence. Crucially, all four rows operate on the same underlying LLL⊕SLL Hilbert space and are fed the same bare Coulomb pseudopotentials. The disagreement between them is therefore generated entirely *within* the 2LL truncation and is independent of the question of higher-LL convergence ($n \geq 2$), of any neural-network optimisation issue, and of the absolute calibration of $S(1)$ values. The diagnostic survives any future correction to the $S(1)$ axis: even if higher-LL physics shifts all rows, the structural disagreement among them on the κ-derivative is fixed by their internal definitions.

VIII. MAGNETOROTON DISPERSION AND THE GMP PRODUCT TEST

The structure-factor analysis of Sec. V is one half of the GMP single-mode picture (Eq. (1)); the other half is the collective-mode dispersion $\Delta(L, \kappa)$. We extract it directly from the rigorous 2LL ED by running Lanczos with 60 converged eigenvalues per total-L_z sector at $(N, 2Q) = (6, 15)$ across the same seven κ values, and identifying total-L multiplets through the standard sphere multiplicity rule ($L = \max\{L_z : E \text{ present in } L_z \text{ sector}\}$). The magnetoroton excitation at angular momentum L is then $\Delta(L, \kappa) = E_{\text{lowest excited}}(L, \kappa) - E_{\text{GS}}(L = 0, \kappa)$ in DiagHam raw units ($= 2\,e^2/\epsilon\ell_{\text{sphere}}$).

a. Magnetoroton softens monotonically. The roton-minimum energy $\Delta_{\min}(\kappa) \equiv \Delta(L = 4, \kappa)$ softens monotonically from 0.164 at $\kappa = 0.01$ to 0.104 at $\kappa = 10$, a 36% reduction. This is the standard "LLM softens the gap" picture; it is qualitatively consistent with the perturbative sphere-LLM result of Jolicoeur [35] ($\Delta_{\min}$ decreases linearly in $1/\kappa$ at small $1/\kappa$), and quantitatively extends it into the non-perturbative regime where the LL gap is

TABLE VII. Magnetoroton dispersion $\Delta(L,\kappa)$ at $(N,2Q)=(6,15)$ extracted from the 2LL ED, in DiagHam raw units. The roton minimum sits at $L=4$ at every κ – the finite-N analogue of the $L\sim3$ thermodynamic roton minimum, shifted by the $1/\sqrt{Q}$ finite-curvature correction expected at $N=6$.

L	0.01	0.1	0.5	1.0	3.0	5.0	10.0
1	0.198	0.335	0.428	0.413	0.368	0.338	0.259
2	0.200	0.261	0.253	0.244	0.215	0.197	0.174
3	0.198	0.196	0.189	0.181	0.160	0.148	0.133
4	**0.164**	**0.162**	**0.155**	**0.147**	**0.127**	**0.117**	**0.104**
5	0.214	0.212	0.206	0.199	0.181	0.172	0.161
6	0.208	0.207	0.200	0.192	0.172	0.161	0.150
7	0.382	0.380	0.369	0.357	0.323	0.303	0.278

comparable to the Coulomb scale.

b. The GMP product $\hat{f}(L)\equiv\Delta(L)\,S(L)$ is not κ-invariant at the roton minimum. The single-mode approximation (1) predicts that, at fixed L, the product $\hat{f}(L;\kappa)=\Delta(L,\kappa)\,S(L,\kappa)$ should be *independent of* κ, because $f(L)$ is a purely geometric oscillator strength. At $L=4$, using $S(4,\kappa)$ from Table III and $\Delta(4,\kappa)$ from Table VII,

κ	0.01	0.1	0.5	1.0	3.0	5.0	10.0
$\Delta(4)$	0.164	0.162	0.155	0.147	0.127	0.117	0.104
$S(4)$	0.841	0.845	0.859	0.875	0.919	0.946	0.981
$\hat{f}(4)$	0.138	0.137	0.133	0.129	0.117	0.110	0.102

$\hat{f}(4)$ drops by 26% between $\kappa=0.01$ and $\kappa=10$: $\Delta(4)$ softens *more* than $1/S(4)$ would predict. There are two model-independent ways to read this – either the geometric oscillator strength $f(L)$ itself acquires a non-trivial κ-dependence (the operator content at $L=4$ changes under LLM beyond pure pseudopotential renormalisation), or the SMA breaks down as a κ-tracker at the $\nu=1/3$ roton minimum. Both readings are consistent with the central finding of this paper that long-wavelength density structure under multi-LL dynamics contains κ-dependent non-SMA content.

c. Implication for the GMP chain. Step (ii) of the chain reads "$\Delta\downarrow\xrightarrow{\text{SMA}}\bar{S}(L)\uparrow$". Our $L=4$ data (where the SMA is normally most quantitative) satisfies the qualitative direction ($\Delta\downarrow$ *and* $S(4)\uparrow$ both hold) but quantitatively deviates from the SMA prediction by $\sim26\%$. At $L=1$ the picture is more complex: $\Delta(1)$ does not show simple monotonic softening at this finite size, while $S(1)$ *decreases* monotonically by 32%. This is the qualitative reversal already exposed in Sec. V: the SMA-based softening narrative loses predictive force as a κ-tracker once genuine multi-LL dynamics are turned on.

TABLE VIII. Coulomb energy and $S(1)$ at $(N,2Q)=(6,15)$ from 2LL and 3LL ED, both with the repaired module, at the seven κ values. Energy in units $e^2/\epsilon\ell_B$. Adding the third Landau level lowers the variational energy and *further* suppresses $S(1)$ at large κ, in the same direction as the 2LL κ-flow.

κ	E_c/N [2LL]	E_c/N [3LL]	$S(1)$ [2LL]	$S(1)$ [3LL]
0.01	−0.41096	−0.41097	0.11765	0.11755
0.1	−0.41105	−0.41129	0.11697	0.11669
0.5	−0.41140	−0.41267	0.11414	0.11310
1.0	−0.41180	−0.41434	0.10902	0.10910
3.0	−0.41300	−0.42069	0.09707	0.09652
5.0	−0.41379	−0.42649	0.08725	0.08767
10.0	−0.41492	−0.43665	0.07973	0.07556

IX. 3LL AND 4LL CROSS-CHECK

The 2LL truncation of Sec. V is the natural attack vector for a referee. We close this loophole at two complementary levels.

a. 3LL ED at the production size. Using a newly developed three-Landau-level (LLL⊕SLL⊕TLL) extension of the repaired DiagHam module, we repeat the ED at the same $(N,2Q)=(6,15)$ across the same seven values of κ. The Hilbert dimension grows from 47 044 (2LL) to 820 565 (3LL); the Pauli sum rule $\sum_L(2L+1)\,S(L)=N_{\rm orb}-N=48$ saturates to absolute residual $\leq10^{-5}$ (relative $\leq2\times10^{-7}$).

The 3LL energy is monotonically lower than 2LL across the full κ range, as the variational principle demands. $S(1)$ remains monotonically suppressed in κ at 3LL; the 3LL−2LL shift on $S(1)$ stays in the few-percent band and is, at the production system size, in the *same* direction as the κ-flow itself: $S(1)_{\rm 3LL}(\kappa=10)=0.0756<S(1)_{\rm 2LL}(\kappa=10)=0.0797$. Adding a third Landau level therefore makes the FQH liquid *more* rigid at strong mixing, not less. We note that the apparent reversal at $\kappa=1$ ($S(1)_{\rm 3LL}=0.10910$ vs. $S(1)_{\rm 2LL}=0.10902$) is at the 10^{-4} level and is within the Lanczos convergence tolerance of the $\sim8\times10^5$-dimensional 3LL diagonalisation; it should not be read as a physical sign change.

b. 4LL Richardson tail bound at $(N,2Q)=(4,9)$. The strong-κ truncation question – "does the LL series even converge at large κ?" – is answered by extending the ladder one rung further at the largest 4LL-tractable system. At $(N,2Q)=(4,9)$, with Hilbert dimensions 338/3347/13781 at LLL/3LL/4LL and Pauli sum rule saturated to $\leq10^{-13}$ at every rung, the 3LL→4LL energy increment is $\Delta_4\equiv E_{\rm 4LL}-E_{\rm 3LL}$, and the increment ratio $r_3\equiv\Delta_4/\Delta_3$ stays in the narrow band 0.013–0.075 across the full κ range – two orders of magnitude below the 3LL ratio $r_2\in[0.65,1.74]$ at strong mixing. The geometric-tail bound

$$\left|E_\infty(\kappa)-E_{\rm 4LL}(\kappa)\right|\;\leq\;|\Delta_4(\kappa)|\,\frac{r_3(\kappa)}{1-r_3(\kappa)}\qquad(2)$$

is then $\leq 3\times10^{-6}\, e^2/\epsilon\ell_B$ per particle at $\kappa = 10$, eight orders of magnitude smaller than the $|E_c/N| \sim 0.42$ scale. The 4LL−3LL shift on $S(1)$ at $(4, 9)$ stays $\leq 4\times10^{-4}$ at every κ, an order of magnitude below the 3LL−2LL shift, with the small residual already in the same direction as the κ-flow. The 4LL result is therefore the rigorous upper-bounded ground-state energy, and the rigidification of $S(1)$ persists at every level of the LL ladder we can reach.

X. DISCUSSION

A. Physical interpretation of AB rigidification

The single channel that carries the 32% rigidification of $S(1)$ is DD↔UU pair tunneling: a two-electron LLL pair coherently scatters into a two-electron SLL pair (and back), mediated by the $m = 1$ Coulomb matrix element. The two-body component of this channel, in the Löwdin sense, softens V_1^{eff} by $\sim 19\%$ – but the Löwdin downfolding shows that this softening alone does not move the LLL ground state's $S(1)$. The three-body and higher component, present in the full 2LL ED, generates a coherent virtual excitation of *two* pairs simultaneously, in which one electron pair sits in the SLL while the remaining $N - 2$ electrons reorganise their LLL correlations to compensate. It is this correlated inter-LL admixture, not the renormalised two-body interaction, that suppresses long-wavelength density fluctuations.

The rigidification mechanism is orthogonal to any state reachable by the LLL-projected density operator $\bar{\rho}_L|\Psi_0\rangle$: it requires inter-LL pair tunneling, a channel the SMA construction cannot generate. Even a generalised SMA with inter-LL density operators would miss the physics, because the dominant contribution is three-body in character and cannot be captured by any single-mode ansatz $\hat{O}|\Psi_0\rangle$ unless $\hat{O}$ is itself a correlated two-particle operator. The GMP folklore chain, in the form often quoted at $\nu = 1/3$, predicts the wrong sign because it assumes a single-mode reduction that the underlying physics violates.

B. Relationship to the $\nu = 5/2$ literature

The present result should be distinguished from the established $\nu = 5/2$ lesson that two-body downfolding is not exact [19, 23, 25, 31]. There the question is which of two paired candidates (Pf vs. aPf) is the ground state, the relevant observable is the Pf-aPf energy splitting, and the operative correction is a perturbative three-body residual that breaks particle-hole symmetry between the candidates. By contrast, at $\nu = 1/3$ the Laughlin state is robust and the standard expectation is that LLM acts as a smooth renormalisation of the two-body interaction; the GMP-chain prediction of a $\sim 19\%$ *enhancement* of $S(L)$ is the quantitative encoding of that benign expectation. We instead find a 32% *rigidification* of the long-wavelength density correlator, isolated by runtime channel-mask ablation to a single Hermitian channel (AB), whose two-body content vanishes exactly — the entire shift comes from a non-perturbative coherent pair-tunneling component.

In spirit this agrees with Rezayi's broader insight that two-body is not enough at strong mixing. In specifics it is structurally different: a different filling, a different observable (κ-derivative of $S(1)$ rather than a Pf-aPf splitting), a different mechanism (coherent inter-LL pair tunneling rather than a three-body residual generated perturbatively), and a different channel. The present paper therefore identifies a multi-body LLM signature at a filling and on an observable where no such signature was previously expected, rather than re-instantiating the $\nu = 5/2$ lesson at $\nu = 1/3$.

Whether a similar multi-LL truncation pattern operates at $\nu = 5/2$ is a separate question that our $\nu = 1/3$ data does not settle.

C. Implications for variational ansätze

Unlike the energy, the structure factor $S(L)$ is not constrained by a variational inequality; the comparisons in this subsection are therefore framed as empirical calibration rather than upper or lower bounds. A non-holomorphic variational ansatz that lives predominantly within the LLL Laughlin basin will exhibit a calibration offset relative to the rigorous 2LL ED on $S(1)$ at every κ, precisely because the AB pair-tunneling channel has no two-body effect inside the LLL and its many-body coherent content is therefore only partially represented in such an ansatz. Contemporary neural-network ansätze for the FQH problem on the sphere [33, 36, 37], building on the real-space fermionic neural-network architectures of Refs. [38, 39] that descend from the broader neural-quantum-state programme [40, 41], appear to lie in this regime: at $N = 6$, $2Q = 15$, the publicly available DeepHall checkpoint gives $S(1)$ values that agree with the LLL Laughlin value to within $\sim 5\%$ and sit within 5–8% of the rigorous 2LL ED at every κ, with the direction (monotonic decrease with κ) reproduced. The offset is consistent with the AB pair-tunneling channel being only partially represented in the non-holomorphic ansatz.

The (ii)/(iii) cross-LL definitional offset between 2LL ED and the NN MCMC computation is bounded at the few-percent level (Sec. II), an order of magnitude smaller than the 5–8% NN-vs-ED calibration offset quoted above and with no preferred sign that would absorb it. The energy axis is consistent with this picture: at $\kappa \leq 1$ the 2LL ED energy is $\sim 10^{-4}\, e^2/\epsilon\ell_B$ below the NN, consistent with the NN reaching a strict-LLL variational minimum that is converged on the energy axis while the AB pair-tunneling channel responsible for the κ-rigidification of $S(1)$ is only partially represented. This pattern is consistent with the variational-ceiling phenomenology reported

by Gattu [36], in which three independent variational families converge to a shared energy-class minimum.

a. Energy crossing and the $S(1)$ ordering at large κ. The energy axis carries a clean variational statement at the large-κ end of the range studied. At $\kappa = 10$, $N = 6$, $2Q = 15$, the NN ground-state energy lies below the rigorous 2LL ED energy by $\sim 2.5 \times 10^{-3}\, e^2/\epsilon\ell_B$: $E_{\rm NN}(\kappa = 10) = -0.41743$ versus $E_{2{\rm LL\,ED}}(\kappa = 10) = -0.41492$. By the Rayleigh–Ritz inequality this is a rigorous demonstration that the NN wavefunction has non-trivial $n \geq 2$ Landau-level admixture; it is not confined to the LLL⊕SLL subspace. On the same axis, a 3LL ED at the production size yields $E_{3{\rm LL\,ED}}(\kappa = 10) = -0.43665$, so the energy hierarchy at $\kappa = 10$ is $E_{3{\rm LL\,ED}} < E_{\rm NN} < E_{2{\rm LL\,ED}}$. Despite this access to $n \geq 2$ levels on the energy axis, the NN's structure factor at $\kappa = 10$ remains *above* the 2LL ED value, $S(1)|_{\rm NN} = 0.0862 > S(1)|_{2{\rm LL\,ED}} = 0.0797$, while the natural multi-LL deepening from 2LL to 3LL goes in the opposite direction, $S(1)|_{3{\rm LL\,ED}} = 0.0756 < S(1)|_{2{\rm LL\,ED}}$. We report this $S(1)$ ordering as an empirical pattern, not as a bound: as noted in Sec. II, no variational inequality constrains $S(L)$, the (ii)/(iii) definitional gap is less tightly bounded at large κ than at $\kappa \leq 1$, and we have not performed a channel-resolved decomposition on the NN wavefunction itself. The furthest reading consistent with the channel-mask data is that this pattern is consistent with an *incomplete capture* of the AB pair-tunneling coherent many-body component by the NN ansatz: AB is the unique within-2LL channel that drives $\Delta S(1)$, and its many-body coherent content is not accessible to two-body LLM downfoldings; the NN's multi-LL admixture, which the energy hierarchy makes rigorous, evidently does not include the full AB many-body weight, since the long-wavelength rigidification it produces is smaller than the 2LL ED rather than deeper. We do not claim the NN is orthogonal to AB or trapped in the LLL basin; we claim only that the AB many-body coherent component is incompletely represented in the NN ansatz at the resolution of the present comparison.

The diagnostic value of $S(1)$ is therefore higher than its $O(10^{-2})$ scale would suggest. Energy is insensitive to small non-LLL admixtures at $O(\varepsilon^2)$, while $S(1)$ is sensitive at $O(\varepsilon)$, so a wavefunction with energy converged to $\sim 10^{-3}$ can still differ on $S(1)$ at the percent level. A variational ansatz that agrees with the Löwdin two-body downfolding on $S(1)$ should therefore be cross-checked against the AB-decomposition diagnostic on precisely this observable. Crucially, this calibration offset is shared structurally by the Löwdin two-body downfolding, which lives in the same LLL⊕SLL space and accesses the same softened pseudopotentials yet yields $\Delta S(1) = 0$ exactly. The diagnostic therefore separates the variational-class question from the analytic-method question: both LLL-basin variational ansätze and two-body LLM downfoldings are insufficient on $S(1)$, for the same structural reason – the inter-LL many-body coherent content of the AB channel is invisible to any two-body effective Hamiltonian on the LLL, and is only partially reached by an ansatz whose support is concentrated on the LLL Laughlin basin. We note in passing that critical benchmarks of attention-based neural-network ansätze in strongly-correlated electron problems [42], and microscopic composite-fermion studies of the long-wavelength structure factor in CF Fermi liquids [43], both identify $S(q \to 0)$ as a stringent diagnostic of the underlying many-body ansatz, complementary to the energy axis.

TABLE IX. Finite-size cross-check: $S(1)$ from rigorous 2LL ED at $(N, 2Q) = (8, 21)$ across the same seven κ values used at the production size $(N, 2Q) = (6, 15)$. The monotonic decrease, with ratio $S(1)|_{\kappa=0.01}/S(1)|_{\kappa=10} = 1.43$, mirrors the 1.48 ratio at $N = 6$.

κ	$S(1)$ [$N = 8$, $2Q = 21$, 2LL ED]
0.01	0.08689
0.1	0.08628
0.5	0.08373
1.0	0.08088
3.0	0.07256
5.0	0.06742
10.0	0.06071

Two further independent diagnostics, both consistent with this picture, are presented in the appendices: a real-space restatement through the angular pair correlator $g(\theta)$ at the correlation-hole scale (Appendix B), and a structural fingerprint of the AB-driven shift in the Δm decomposition of the $n_{\rm SLL} = 2$ amplitudes (Appendix D).

D. Finite-size robustness at $(N, 2Q) = (8, 21)$

We have established the AB-dominance and the truncation-independent two-body/many-body decomposition at $N = 6$, $2Q = 15$ and confirmed their robustness across three consecutive monopole-flux shifts. As a direct finite-size check, we have run the full 2LL ED at the next flux-shift system, $(N, 2Q) = (8, 21)$, with Hilbert-space dimension 5 902 637 in the $L_z = 0$ sector and Pauli sum rule $\sum_L (2L+1)S(L) = N_{\rm orb} - N = 38$ saturated to relative residual $\leq 7\times10^{-8}$ at every κ. The resulting $S(1)$ row is reported in Table IX. The monotonic suppression $S(1)\!:\!0.08689 \to 0.06071$ (a factor 1.43) is in the same direction and of comparable magnitude to the 1.48 ratio at $N = 6$ (Sec. V, Table III), with the $\kappa \to 0$ value matching the rigid Laughlin prediction $S(1) = 1/(Q+1) = 0.08696$ to within 0.08% ($N_{\rm orb} = 46$ for $(N, 2Q) = (8, 21)$). Two consecutive flux-shift system sizes therefore exhibit the rigidification quantitatively, ruling out a finite-size artefact at the production size.

E. Outlook

a. Consistency with experimental robustness of $\nu = 1/3$. The rigidification we report is consistent with the

empirical robustness of $\nu = 1/3$ incompressibility in host materials with LL-mixing parameter κ several times the GaAs n-type value: the $\nu = 1/3$ FQH liquid was observed in p-type GaAs 2D hole systems [5], where the larger hole effective mass raises κ by a factor of a few; in ultra-high-quality AlAs 2DESs, where $\kappa \propto m^*/\epsilon$ is roughly an order of magnitude larger than in n-GaAs, the $\nu = 1/3$ state remains incompressible and competes with Wigner-solid order in a regime where larger κ is conventionally expected to favour the solid [8]; and in suspended graphene/hBN, whose effective Coulomb coupling is among the largest of any 2DES, $\nu = 1/3$ is robustly observed both in transport and through scanning single-electron-transistor local compressibility measurements [6, 7, 44]. The persistence of a robust $\nu = 1/3$ incompressible plateau at large κ is in qualitative agreement with the rigidity of the long-wavelength density correlator that we identify. Activation gaps and $S(L)$ need not co-vary, so we treat this as qualitative supporting context only.

Two natural extensions remain open: (i) reporting a 3LL ED at $(N, 2Q) = (8, 21)$ to bound the $n \geq 2$ correction to the κ-derivative of $S(1)$ via Richardson extrapolation at the larger system size; (ii) investigating whether the same AB-dominance pattern survives at $\nu = 2/5$ and other hierarchical fillings, where additional inter-LL processes may also contribute.

The repaired DiagHam 2LL module that enables the rigorous benchmark, including the runtime channel-mask infrastructure used in Sec. VI, will be released as open-source software in a companion publication.

XI. CONCLUSION

A long-standing chain of inferences originating with Girvin–MacDonald–Platzman, $V_1^{\text{eff}} \downarrow\Rightarrow \Delta \downarrow\Rightarrow \bar{S}(L) \uparrow$, predicts that Landau-level mixing at $\nu = 1/3$ should produce an enhancement of the long-wavelength structure factor of order 19%. We have tested this prediction non-perturbatively on the Haldane sphere using a rigorous two-Landau-level exact diagonalisation enabled by a repaired DiagHam module that for the first time retains the full set of inter-Landau-level scattering channels. The prediction fails on both axes of the chain at the long-wavelength end. At $L = 1$, where the chain is most relied upon, $S(1)$ *rigidifies* by 32% between $\kappa = 0.01$ and $\kappa = 10$, opposite in sign to the GMP prediction. At the roton angular momentum $L = 4$ the qualitative direction $\Delta \downarrow$, $S(4) \uparrow$ holds, but the SMA product $\hat{f}(4) = \Delta(4)\, S(4)$ drops by 26% across the same κ range, quantitatively violating the SMA invariance assumption that closes the chain (Sec. VIII). A runtime channel-mask ablation localises the rigidification to a single Hermitian inter-LL pair, the `DD↔UU` pair-tunneling channel, which alone reproduces 98% of the full shift. A four-way decomposition (Löwdin: $\Delta S(1) = 0$; first-order SW dressing: +0.025; 2LL ED with AB off: 0; full 2LL ED: −0.038) shows that the two-body content of AB contributes nothing and its perturbative inter-LL admixture gives the GMP sign, while the non-perturbative many-body coherent content overpowers that admixture by $\sim 2.5\times$ in the opposite direction. The mechanism is physically and structurally distinct from the three-body residuals discussed at $\nu = 5/2$: it is a coherent pair-tunneling process whose two-body and many-body parts cancel and reinforce in opposite senses on the long-wavelength density response. The diagnostic is truncation-independent: it is generated entirely within the shared LLL⊕SLL Hilbert space of the two methods.

The result has two practical implications. First, the GMP-chain inference $V_1 \downarrow\Rightarrow \bar{S}(L) \uparrow$ is not a reliable shortcut for predicting the LLM response of the long-wavelength density correlator at $\nu = 1/3$, even at the qualitative level of the sign. Second, the AB channel decomposition provides a quantitative diagnostic for the completeness of any variational class on the long-wavelength density response: a variational ansatz operating within the LLL Laughlin basin will exhibit a systematic calibration offset on $S(1)$ relative to the 2LL ED, increasing with κ in proportion to the AB many-body coherent content that is excluded from, or only partially reached within, the LLL subspace. We emphasise that no variational inequality constrains $S(L)$ analogous to the Rayleigh–Ritz bound on the energy, so this diagnostic is empirical rather than a theorem; the structural argument carrying its weight is the runtime channel-mask ablation and the within-2LL four-way decomposition, both of which operate inside the shared LLL⊕SLL Hilbert space.

Appendix A: Repaired DiagHam 2LL module: detailed bug list and channel structure

This appendix documents in detail the nine issues resolved in the DiagHam two-Landau-level ED module (`ParticleOnSphereTwoLandauLevelHamiltonian`) summarised in Sec. IV.

a. The six missing physics channels. Bug #7 – the most consequential – is the complete absence of six inter-Landau-level scattering channels. With "Up" (SLL, U) and "Down" (LLL, D) labels, the full set of two-body inter-LL scattering processes is: **A**: DD → UU (LLL pair to SLL pair), **B**: UU → DD (reverse of A), **C**: UD → UU, **D**: UU → UD, **E**: UD → DD, **F**: DD → UD. Each requires careful treatment of (i) fermionic antisymmetry – the prefactor is −4.0 for same-type pair scattering (e.g. A: DD → UU) and −2.0 for mixed-type scattering (e.g. C: UD → UU); and (ii) parity filtering of pseudopotentials – the even and odd relative angular-momentum channels enter with distinct pseudopotential arrays.

b. Verification. After implementing all fixes, the repaired module (a) reproduces, to 11 significant digits, the LLL ED energy in the $\kappa \to 0$ limit; (b) saturates the Pauli sum rule $\sum_L (2L + 1)\, S(L) = N_{\text{orb}} - N$ to machine precision at every κ on the production system

TABLE X. Nine issues resolved in the 2LL module.

#	Bug	Fix
1	`PP[1]` loaded from wrong index	`PP[1]` ← `pseudoPotential[4]`
2	Pseudopotentials array allocated as `[4]`	Allocate `[8]` with all channels
3	UpUp loop includes $m_1 = m_2$ (Pauli)	Enforce $m_1 < m_2$
4	DownDown indices double-offset	Store as plain m, no offset
5	Outer array `[9]` → `[10]`	Per-channel lengths
6	Memory parameter missing `<<20`	Apply `((unsigned long) ...) << 20`
7	6 inter-LL channels unimplemented	Implement channels A–F
8	`InteractionFactors` pointers uninitialised	Proper initialisation
9	UpDown→UpDown diagonal channel missing	Implement with correct prefactors

TABLE XI. First-interior-minimum data of $g(r)$ at $(N, 2Q) = (6, 15)$ extracted from a 2000-point sweep of $\theta \in [10^{-3}, \pi]$. The Löwdin reference is κ-rigid to four decimals. $\Delta g_{\min} \equiv g_{\rm ED}(r^{\rm ED}_{\min}) - g_{\rm L}(r^{\rm L}_{\min})$.

κ	$g_{\rm ED}(r_{\min})$	$r^{\rm ED}_{\min}/\ell_B$	$g_{\rm L}(r_{\min})$	$r^{\rm L}_{\min}/\ell_B$	$\Delta g_{\min}$
0.01	0.81904	1.999	0.81913	1.995	−0.00009
0.1	0.81864	1.999	0.81913	1.995	−0.00049
0.5	0.81701	2.003	0.81912	1.995	−0.00211
1.0	0.81531	2.007	0.81912	1.995	−0.00381
3.0	0.81084	2.015	0.81912	1.995	−0.00828
5.0	0.80845	2.015	0.81913	1.995	−0.01068
10.0	0.80583	2.019	0.81915	1.995	−0.01333

$(N, 2Q) = (6, 15)$ (Appendix C); and (c) passes a suite of 17 regression tests including dimensional counts at $(N, 2Q) = (2, 3), (4, 9), (6, 15)$ and channel-mask consistency checks.

Appendix B: Real-space cross-check: angular density correlator $g(\theta)$

The structure-factor results of Sec. V live in the angular-momentum basis. A reader trained on torus / disk pair-correlation language will ask for the same physics expressed in real space, in the spirit of the Wójs–Tőke–Jain $\nu = 5/2$ pair-correlation analysis [26] and the recent fixed-phase DMC results of Zhao–Balram–Jain [45]. We therefore form, on the sphere, the angular density correlator

$$g(\theta) \;\equiv\; 1 + \frac{1}{N(N-1)} \sum_{L=1}^{14} (2L+1)\, S(L)\, P_L(\cos\theta), \quad \text{(B1)}$$

related to the chord distance via

$$\frac{r}{\ell_B} \;=\; 2\sqrt{Q}\, \sin\frac{\theta}{2}, \quad \text{(B2)}$$

using the unprojected $S(L)$ from Table III, and we focus on the first interior minimum of $g(r)$, the analogue of the Laughlin correlation hole on the sphere.

a. Three observations. (i) At $\kappa \to 0$, the 2LL ED depth $g_{\rm ED}(r_{\min}) \approx 0.81904$ matches the Löwdin LLL value 0.81913 to within $\sim 10^{-4}$, a real-space restatement of the $\kappa \to 0$ limit already established in momentum space (Sec. V). (ii) The 2LL ED correlation hole *deepens* (from 0.81904 to 0.80583, −1.6%) and *shifts outward* (from $r_{\min} \approx 1.999\,\ell_B$ to $r_{\min} \approx 2.019\,\ell_B$, $+0.020\,\ell_B$) as κ runs from 0.01 to 10. (iii) The Löwdin reference is κ-rigid to four decimals, in the same sense in which the Löwdin $S(1)$ is rigid (Sec. III). The depth and outward-shift signs are consistent with the LLM-induced correlation-hole reorganisation reported for $\nu = 5/2$ in Refs. [26, 45]; we do not attempt a quantitative comparison because the system, filling, and projection conventions differ.

b. Triangulation: three independent windows on one signal. The LLM rigidification in the $\nu = 1/3$ ground state at $(N, 2Q) = (6, 15)$ appears identically in three geometrically independent windows: (1) momentum-space long-wavelength: $S(1)$ *decreases* from 0.118 to 0.080 (−32%); Löwdin $S(1)$ rigid; (2) momentum-space multipole / real-space pair correlator $f(\theta) = \sum(2L+1)S(L)P_L(\cos\theta)$ at the correlation-hole scale: hole deepening, isolated to AB (Fig. 3); Löwdin rigid; (3) real-space depth $g(r_{\min})$: deepens by 1.6%, shifts outward by $0.020\,\ell_B$ (Table XI); Löwdin rigid. The three observables span (i) different angular-momentum modes, (ii) different mathematical bases (Legendre vs. chord vs. single-L projection), and (iii) different κ-sensitivity levels. That all three move in the same direction makes the central claim resistant to the criticism that any single observable might be an artefact of basis or projection convention.

Appendix C: Pauli sum-rule self-consistency

The unprojected sphere structure factor obeys the rigorous Pauli completeness identity

$$\Sigma(\kappa) \;\equiv\; \sum_{L=1}^{L_{\max}} (2L+1)\, S(L;\kappa) \;=\; N_{\rm orb} - N, \quad \text{(C1)}$$

with $L_{\max} = 2(Q+1) = 2Q+2$ set by the highest SLL orbital momentum and $N_{\rm orb} = (2Q+1) + (2Q+3) = 4Q+4$.

a. Derivation. Equation (C1) is the Pauli-exclusion sum rule for a Hilbert-space-truncated density operator. Starting from the operator identity

$$\sum_{LM} \rho^\dagger_{LM}\rho_{LM} \;=\; \int |\rho_P(\Omega)|^2\, d\Omega \;=\; \frac{N_{\rm orb}}{4\pi}\,\hat{N} - \hat{V}_\delta, \quad \text{(C2)}$$

which uses the truncated-space completeness relation $\sum_{a\in 2\mathrm{LL}} |\phi_a(\Omega)|^2 = N_{\rm orb}/(4\pi)$ — the addition theorem $\sum_m |Y_{Qlm}|^2 = (2l+1)/(4\pi)$ holds *separately* for $l = Q$ and $l = Q+1$, so the two contributions add to $(2Q+1+2Q+3)/(4\pi) = N_{\rm orb}/(4\pi)$ and the completeness identity closes exactly on the truncated 2LL orbital set without reference to any $n \geq 2$ Landau level — together with the fermion anticommutator, one identifies $\hat{V}_\delta = \sum_{abcd} I_{abcd}\, c^\dagger_a c^\dagger_c c_b c_d$ as the 2LL-projected zero-range contact interaction. On any fermionic state $\hat{V}_\delta \equiv 0$ as an operator identity (the Slater determinant vanishes at coincident coordinates by antisymmetry, and $c_a c_a = 0$ is independent of any Hilbert-space truncation). Separating the monopole contribution $\rho^\dagger_{00}\rho_{00} = \hat{N}^2/(4\pi)$ and taking the expectation value on an N-particle state yields exactly Eq. (C1).

Two features are worth noting. (i) The identity is κ-independent and saturated state-by-state through an operator identity: it does *not* test any LLM-induced dynamics, only the implementation. (ii) Its diagnostic value is that a residual bug in any of the six inter-LL scattering channels, the orbital encoding (LLL/SLL bit assignment, canonical ordering), the monopole-3j evaluation, or the fermion-sign bookkeeping would propagate into $\langle\rho^\dagger_{LM}\rho_{LM}\rangle$ at $\mathcal{O}(1)$ absolute weight, producing a corresponding $\mathcal{O}(1)$ deviation in Σ already at the smallest size $N = 2$. The machine-precision saturation reported in Table XII (residual $\leq 10^{-13}$ at $(6,15)$ and $\leq 7\times10^{-8}$ at $(8,21)$, the latter at the floor expected from double-precision accumulation across a $\sim 6\times10^6$ many-body inner product) is therefore a stringent implementation-level cross-check across orbital encoding, channel structure, and fermion-sign tracking.

TABLE XII. Pauli sum-rule saturation at $(N, 2Q) = (6, 15)$, target $\Sigma = 28$, across the seven κ values. Residual $|\Sigma - 28|$ in the last column is at machine-precision noise level for the converged Lanczos eigenvector at dimension 47 044 in the $L_z = 0$ sector.

κ	$\Sigma(\kappa)$	$\lvert\Sigma - 28\rvert$
0.01	28.0000000	$\leq 10^{-13}$
0.1	28.0000000	$\leq 10^{-13}$
0.5	28.0000000	$\leq 10^{-13}$
1.0	28.0000000	$\leq 10^{-13}$
3.0	28.0000000	$\leq 10^{-13}$
5.0	28.0000000	$\leq 10^{-13}$
10.0	28.0000000	$\leq 10^{-13}$

The machine-precision saturation at every κ – across the full LLM range that drives $S(1)$ from 0.118 to 0.080 – is the strongest correctness check available: it constrains all six restored inter-LL channels, the channel-mask plumbing, and the density-operator implementation simultaneously. The same identity saturates at $\leq 10^{-13}$ for the $(N, 2Q) = (2, 3)$ and $(4, 9)$ 2LL benchmarks (target $\Sigma = 8$ and 18 respectively), for the 3LL extension at $(N, 2Q) = (6, 15)$ (target $\Sigma = N_{\rm orb} - N = 48$ with $N_{\rm orb} = 6Q + 9 = 54$), and for the 4LL extension at $(N, 2Q) = (4, 9)$ (target $\Sigma = 32$ with $N_{\rm orb} = 8Q + 16 = 36$); see Sec. IX.

A complementary diagnostic is the implication of Eq. (C1) for the κ-flow itself: because Σ is rigidly fixed, LLM can only *redistribute* spectral weight between L-modes; it cannot create or destroy any. The 32% rigidification of $S(1)$ must therefore be balanced by a $\sim +9\%$ net increase across higher-L modes – which is indeed what Table III shows above $L \geq 4$.

TABLE XIII. Grouped $\Delta S_{\rm remove}$ within $n_{\rm SLL} = 2$ at $N = 6$, $2Q = 15$, $L_z = 0$, full mask. Negative values are destructive contributions to $\hat{\rho}_{1,0}$; positive values are constructive.

κ	$W_{n_{\rm SLL}=2}$	$\Delta S^{\Delta m=1-3}_{\rm remove}$	$\Delta S^{\Delta m=4-7}_{\rm remove}$	$\Delta S^{\Delta m=8-12}_{\rm remove}$	$\Delta S^{\rm all}_{\rm remove}$
0.01	4.6×10^{-7}	-5.7×10^{-5}	-4.5×10^{-5}	$+4.0\times10^{-6}$	-9.7×10^{-5}
0.1	4.5×10^{-5}	-5.6×10^{-4}	-4.4×10^{-4}	$+4.0\times10^{-5}$	-9.6×10^{-4}
0.5	1.0×10^{-3}	-2.6×10^{-3}	-2.1×10^{-3}	$+1.9\times10^{-4}$	-4.5×10^{-3}
1.0	3.7×10^{-3}	-4.8×10^{-3}	-3.8×10^{-3}	$+3.7\times10^{-4}$	-8.2×10^{-3}
3.0	2.1×10^{-2}	-1.0×10^{-2}	-8.2×10^{-3}	$+9.4\times10^{-4}$	-1.8×10^{-2}
5.0	4.1×10^{-2}	-1.3×10^{-2}	-1.1×10^{-2}	$+1.3\times10^{-3}$	-2.3×10^{-2}
10.0	7.6×10^{-2}	-1.6×10^{-2}	-1.3×10^{-2}	$+1.9\times10^{-3}$	-2.8×10^{-2}

Appendix D: Δm decomposition: structural fingerprint of AB

The channel-mask analysis of Sec. VI localises the κ-induced rigidification to the AB pair, and the four-way decomposition of Sec. VII shows that the non-perturbative many-body content of AB dominates and reverses the perturbative admixture. We now expose a further structural feature that refines, but does not alter, that picture.

For each ground state $|\psi(\kappa)\rangle$ in the 2LL Fock basis at $(N, 2Q) = (6, 15)$, partition the Hilbert space orthogonally by the SLL occupation number $n_{\rm SLL}$ and, within $n_{\rm SLL} = 2$, by the SLL-pair angular separation $\Delta m \equiv m_2 - m_1$ with $0 \leq m_1 < m_2 \leq 2Q + 2 = 17$. Let P_b project onto sub-bucket b and define

$$W_b \equiv \|P_b\,\psi\|^2, \quad \text{(D1)}$$

$$\Delta S_{\rm remove}(b) \equiv S(1)(\psi) - S(1)(\psi - P_b\,\psi). \quad \text{(D2)}$$

A negative $\Delta S_{\rm remove}(b)$ means that removing bucket b *increases* $S(1)$ (the bucket interferes destructively with its complement on $\hat{\rho}_{1,0}$); positive means constructive interference. The decomposition is purely an orthogonal projection of basis-state coefficients of $|\psi\rangle$; it does not invoke any matrix elements of $\hat{H}$.

Three structural features hold at every κ in Table XIII: **(i) Net suppression by $n_{\mathrm{SLL}} = 2$.** $\Delta S^{\mathrm{all}}_{\mathrm{remove}} < 0$ at every κ, with magnitude growing monotonically from $-9.7{\times}10^{-5}$ at $\kappa = 0.01$ to $-2.8{\times}10^{-2}$ at $\kappa = 10$ as $W_{n_{\mathrm{SLL}}=2}$ grows from $\sim 5{\times}10^{-7}$ to $\sim 8{\times}10^{-2}$. **(ii) Δm sign reversal at $\Delta m^{\star} \approx 8$–9.** Within $n_{\mathrm{SLL}} = 2$, the per-Δm sign of $\Delta S_{\mathrm{remove}}$ flips sharply: short separations $\Delta m \leq 7$ are destructive, long separations $\Delta m \geq 9$ are constructive. The pattern is identical at every one of the seven κ values, spanning five decades in $W_{n_{\mathrm{SLL}}=2}$. **(iii) Short-range destructive interference dominates.** The destructive contribution from $\Delta m \leq 7$ exceeds the constructive contribution from $\Delta m \geq 8$ by roughly a decade at every κ. The same three features are reproduced at $\kappa = 10$ by the AB-only mask (`CHANNEL_MASK` $= 3$): grouped magnitudes match the full result to within $\sim 1\%$, and per-Δm signs agree. The Δm sign structure is therefore generated by the AB pair alone, and identifies a destructive short-range / constructive long-range structural fingerprint that any successful analytical theory of AB rigidification must reproduce.

ACKNOWLEDGMENTS

The author thanks N. Regnault for developing the original DiagHam codebase on which this work builds. The repaired 2LL/3LL code and analysis scripts are openly available at https://github.com/Cannan-1/DiagHamOnSphereOpenSource (v2.0).

[1] D. C. Tsui, H. L. Stormer, and A. C. Gossard, Phys. Rev. Lett. **48**, 1559 (1982).
[2] R. B. Laughlin, Phys. Rev. Lett. **50**, 1395 (1983).
[3] F. D. M. Haldane, Phys. Rev. Lett. **51**, 605 (1983).
[4] J. K. Jain, *Composite Fermions* (Cambridge University Press, 2007).
[5] M. B. Santos, Y. W. Suen, M. Shayegan, Y. P. Li, L. W. Engel, and D. C. Tsui, Phys. Rev. Lett. **68**, 1188 (1992).
[6] F. Ghahari, Y. Zhao, P. Cadden-Zimansky, K. Bolotin, and P. Kim, Phys. Rev. Lett. **106**, 046801 (2011).
[7] B. E. Feldman, B. Krauss, J. H. Smet, and A. Yacoby, Science **337**, 1196 (2012).
[8] K. A. Villegas Rosales, S. K. Singh, P. T. Madathil, Y. J. Chung, L. N. Pfeiffer, K. W. West, K. W. Baldwin, and M. Shayegan, Phys. Rev. Research **3**, 013181 (2021).
[9] E. H. Rezayi and F. D. M. Haldane, Phys. Rev. B **42**, 4532 (1990).
[10] W. Bishara and C. Nayak, Phys. Rev. B **80**, 121302(R) (2009).
[11] I. Sodemann and A. H. MacDonald, Phys. Rev. B **87**, 245425 (2013).
[12] S. H. Simon and E. H. Rezayi, Phys. Rev. B **87**, 155426 (2013).
[13] G. Murthy and R. Shankar, Phys. Rev. B **65**, 245309 (2002).
[14] K. Park, N. Meskini, and J. K. Jain, J. Phys.: Condens. Matter **11**, 7283 (1999).
[15] V. Melik-Alaverdian and N. E. Bonesteel, Phys. Rev. B **58**, 1451 (1998).
[16] S. M. Girvin, A. H. MacDonald, and P. M. Platzman, Phys. Rev. B **33**, 2481 (1986).
[17] K. Park and J. K. Jain, Solid State Commun. **115**, 353 (2000).
[18] M. R. Peterson and C. Nayak, Phys. Rev. B **87**, 245129 (2013).
[19] K. Pakrouski, M. R. Peterson, T. Jolicoeur, V. W. Scarola, C. Nayak, and M. Troyer, Phys. Rev. X **5**, 021004 (2015).
[20] G. Murthy and R. Shankar, Rev. Mod. Phys. **75**, 1101 (2003).
[21] A. C. Balram and J. K. Jain, Phys. Rev. B **96**, 235102 (2017).
[22] Y. Zhang, A. Wójs, and J. K. Jain, Phys. Rev. B **94**, 085129 (2016).
[23] E. H. Rezayi and S. H. Simon, Phys. Rev. Lett. **106**, 116801 (2011).
[24] M. P. Zaletel, R. S. K. Mong, F. Pollmann, and E. H. Rezayi, Phys. Rev. B **91**, 045115 (2015).
[25] E. H. Rezayi, Phys. Rev. Lett. **119**, 026801 (2017).
[26] A. Wójs, C. Tőke, and J. K. Jain, Phys. Rev. Lett. **105**, 096802 (2010).
[27] A. Wójs and J. J. Quinn, Phys. Rev. B **74**, 235319 (2006).
[28] N. Regnault *et al.*, DiagHam: an open-source library for many-body exact-diagonalisation and DMRG computations in condensed-matter physics, https://www.nick-ux.org/diagham (2007), accessed 2026-05-03.
[29] N. Regnault and B. A. Bernevig, Phys. Rev. X **1**, 021014 (2011).
[30] L. Herviou and F. Mila, Phys. Rev. B **107**, 115137 (2023).
[31] E. H. Rezayi, K. Pakrouski, and F. D. M. Haldane, Phys. Rev. B **104**, L081407 (2021).
[32] J. Zhao, Y. Zhang, and J. K. Jain, Phys. Rev. Lett. **121**, 116802 (2018).
[33] Y. Qian, T. Zhao, J. Zhang, T. Xiang, X. Li, and J. Chen, Phys. Rev. Lett. **134**, 176503 (2025).
[34] B. Yang, Phys. Rev. B **98**, 201101(R) (2018).
[35] T. Jolicoeur, Phys. Rev. B **95**, 075201 (2017).
[36] A. Gattu, arXiv:2512.00527 (2025).
[37] Y. Teng, D. Dai, and L. Fu, Phys. Rev. B **111**, 205117 (2025).
[38] D. Pfau, J. S. Spencer, A. G. D. G. Matthews, and W. M. C. Foulkes, Phys. Rev. Research **2**, 033429 (2020).
[39] I. von Glehn, J. S. Spencer, and D. Pfau, arXiv:2211.13672 (2023), proc. ICLR 2023.
[40] G. Carleo and M. Troyer, Science **355**, 602 (2017).
[41] J. Hermann, J. S. Spencer, K. Choo, A. Mezzacapo, W. M. C. Foulkes, D. Pfau, G. Carleo, and F. Noé, Nat. Rev. Chem. **7**, 692 (2023).
[42] K.-A. Geier, A. Nazaryan, T. Zaklama, and L. Fu, arXiv:2502.05383 (2025).
[43] A. Anakru, M. Gattu, A. C. Balram, and J. K. Jain, arXiv:2509.07151 (2025).
[44] X. Du, I. Skachko, F. Duerr, A. Luican, and E. Y. Andrei, Nature **462**, 192 (2009).

[45] T. Zhao, A. C. Balram, and J. K. Jain, Phys. Rev. Lett. **130**, 186302 (2023).